Full length article

Ferromagnetism in High Entropy Cantor alloy triggered and tuned by severe plastic deformation

Shabnam Taheriniya [a,*], Reshma Sonkusare [b], Torben Boll [c], Sergiy V. Divinski [a], Martin Peterlechner [d], Harald Rösner [a], Gerhard Wilde [a]

[a] *University of Münster, Institute of Materials Physics, Wilhelm-Klemm-Str. 10, 48149 Münster, Germany*
[b] *Helmholtz-Zentrum Hereon, Institute of Material and Process Design, Max Planck Strasse 1, 21502 Geesthacht, Germany*
[c] *Institute of Applied Materials (IAM-WK), Institute for Nanotechnology (INT) and Karlsruhe Nano Micro Facility (KNMF), Karlsruhe Institute of Technology, 76344 Eggenstein-Leopoldshafen, Germany*
[d] *Karlsruhe Institute of Technology, Laboratorium für Elektronenmikroskopie, Engesserstr.7, 76131 Karlsruhe, Germany*

ARTICLE INFO

ABSTRACT

The process of severe plastic deformation (SPD) introduces unique conditions to materials, leading to the emergence of novel properties. This research specifically investigates the observation of deformation-induced ferromagnetism resulting from SPD processing. High-pressure torsion (HPT) is utilized to process both single-phase and nanocomposite high entropy alloys (HEAs). Vibrating sample magnetometry (VSM) confirms that HPT processing triggers the development of ferromagnetic properties. The distribution and alignment of magnetic domains post-SPD treatment are further examined using differential phase contrast scanning transmission electron microscopy (DPC STEM). Atom probe tomography (APT) analysis suggests that this phenomenon stems from the localized enrichment of ferromagnetic elements, particularly Ni, induced by deformation. This observation underscores the 'cocktail effect' in HEAs, whereby interactions between different elements has led to this unique magnetic behavior. Additionally, deliberate mechanical mixing of the CoCrFeMnNi alloy with a HfNbTaTiZr HEA, comprising non-ferromagnetic constituents, introduces a large rotational strain that alters the ferromagnetic properties. This mixing facilitates a transition from a random orientation of magnetic domains, as seen in the HPT-processed single CoCrFeMnNi alloy, to a coordinated alignment within the nanocomposite HEA.

1. Introduction

Specific functional applications of materials that are fit for the future have elevated the significance of properties such as thermal stability, high strength, low-heat generation, and improved mechanical performance at cryogenic temperature to a paramount level. Various fields, including information storage, superconductivity, electrical power transmission, and high-speed switching or signal transmission, share a common requirement for thermally stable ferromagnetic materials [1]. Consequently, it becomes indispensable to investigate materials that demonstrate exceptional properties across a broad spectrum of operating temperatures. In this context, high entropy alloys (HEAs) stand out as promising candidates for the forthcoming undertakings [2,3]. Due to their high configurational entropy and different local atomic environments, HEAs and compositionally complex alloys exhibit a high potential for application in different aspects of materials science [2,4–11]. In this regard, the emergence of new properties as

a result of the multi-principal alloy design that has been termed as 'cocktail effect' [12,13] seems particularly attractive. Among the four 'core effects' of HEAs, the "cocktail effect", originally introduced by Ranganathan [12], is the most abstract concept. In literature, there are only a few examples demonstrating this effect, which are attributed to the development of new phenomena or properties. For example, Cao et al. [14] attributed strengthening and strain-hardening mechanisms in fcc HEAs at ambient and cryogenic temperatures to the 'cocktail effect'. Being still obscure [15], it was suggested to use this term in relation to the surprising and exotic properties that can arise in HEAs due to their chemical complexity [13]. The 'cocktail effect' becomes even more interesting when elements with different structural, kinetic, and ferromagnetic properties are combined as constituents of a single-phase or nanocomposite HEA. This may give rise to unexpected interactions between the elements and the development of properties or phases beyond what is predicted by the simple rule of mixtures.

* Corresponding author.
  E-mail address: s_tahe01@uni-muenster.de (S. Taheriniya).

In fact, the present study focuses on this very phenomenon. One highly interesting area of research in the field of complex metallic alloys is the phenomenon of deformation-induced ferromagnetism [16]. Certain alloys with equiatomic composition, which are paramagnetic in the un-deformed state, have been found to exhibit ferromagnetic properties after undergoing deformation processes such as rolling or cold-working [17]. This unexpected behavior has been attributed to changes in the local atomic environment and the creation of defects during deformation, leading to the formation of ferromagnetic clusters. Understanding the mechanisms behind deformation-induced ferromagnetism in these alloys could lead to the development of new multifunctional magnetic materials with improved mechanical properties. Furthermore, the ability to precisely control the microstructural components of magnetic materials can unlock new opportunities for designing and fine-tuning high-performance magnets [18–20]. Progress in this field could significantly boost applications in electronics, sensing, and energy conversion, resulting in more efficient and potent technologies.

In our study, we analyze and contrast two distinct methods of inducing ferromagnetism in HEAs. We demonstrate that deformation significantly facilitates atomic migration, leading to the localized accumulation of ferromagnetic elements. This process serves as the fundamental mechanism responsible for the development of ferromagnetism in this material.

2. Materials and methods

2.1. Sample preparation

The single-phase fcc CoCrFeMnNi alloy known as "Cantor" alloy was produced by arc melting of 99.9% purity Co, Cr, Mn, Fe, and Ni pieces in equiatomic proportions in Ar atmosphere. A subsequent homogenization step at 1373 K for 50 h was carried out with the sample sealed in a quartz tube filled with Ar. Throughout the manuscript, this particular sample will be denoted as the as-cast Cantor alloy. The high-pressure torsion (HPT) processed Cantor alloy is a 1 mm thick disk with a diameter of 7.5 mm, cut from the homogenized equiatomic CoCrFeMnNi rod. The HPT processing is carried out under a constant pressure of 9 GPa up to 15 revolutions at ambient temperature at a torsional deformation rate of 1 revolution per minute. To this end, the disk is placed inside anvils each with 0.4 mm deep and 7.5 mm diameter cavities.

For the production of the HEA nanocomposite, forced mechanical mixing of two separate HEA disks was employed. One disk is the single phase fcc CoCrFeMnNi and the other is a single phase bcc HfNbTaTiZr HEA. Both phases were in coarse grained states and had a uniform chemical composition after going through a homogenization step. The elements used for the production of the HfNbTaTiZr alloy, also known as the "Senkov" alloy, were 2–5 μm granules of 99.99% purity and the single-phase bcc solid solution was prepared by arc melting in an argon atmosphere with a final heat treatment process comprising several steps at 1473 K for 48 h under Ar atmosphere. Prior to the HPT processing, the disks were polished down to a thickness of 0.5 mm and the initial diameter was 7.5 mm. One side of the disks was mechanically polished to have a mirror-like finish, and the other side remained rough for better friction between the disks and the anvils. The disks were then stacked on one another and placed between the anvils with a cavity depth of 0.4 mm each (the overall cavity depth was about 0.8 mm). To create a uniform bulk nanocomposite as the final microstructure, the HPT bonding of originally separate disks involved up to 15 revolutions.

2.2. Magnetic property measurements

The characterization of the magnetic properties in the bulk was carried out using a physical property measurement system (PPMS) Evercool II by Quantum Design. The PPMS was set to VSM mode for the

Table 1

VSM hysteresis peak magnetization point at 0.2 T, coercivity and retentivity values recorded at RT and 10 K for the Cantor alloy in different states based on the results shown in Fig. 1.

	as-cast Cantor	HPT Cantor	Nanocomposite HEA
Magnetization at 0.2 T in (J/T) × 10^{-6}			
RT	0.62	1.65	0.59
10 K	1.30	5.03	4.00
Coercivity (kA/m)			
RT	–	1.56	2.61
10 K	8.23	13.50	11.28
Retentivity (J/T) × 10^{-6}			
RT	–	0.077	0.035
10 K	0.096	0.82	0.46

measurement of magnetic properties at RT, as well as at 10 K under pre-vacuum conditions below 10 mbar. Since magnetic properties scale with the sample volume, masses and volumes were chosen to be comparable for all measurements. The average sample mass was 14.5 ± 0.5 mg. All samples had a regular cuboid shape with an average length of 5.3 ± 0.3 mm and an average width of 0.7 ± 0.1 mm. The hysteresis loops were accurately recorded with 2 mm amplitude and 40 Hz frequency for the sample vibration. A magnetic field of 0.2 T (160 kA/m) was applied for the measurements, oriented along the shear direction of the HPT-processed samples or the edge of the cuboid in the case of the un-deformed as-cast sample. In relation to the effect of temperature on the magnetic moments in the HPT-processed or as-cast samples, a temperature sweep series was acquired from 5 K up to 300 K (RT) with 5 K/min while keeping the magnetic field constant at 0.2 T (160 kA/m).

2.3. Differential phase contrast scanning transmission electron microscopy

Differential phase contrast (DPC) is a contrast mechanism used in conjunction with scanning transmission electron microscopy (STEM) to visualize magnetic or electric fields within a transmission electron microscope (TEM) [21–27]. Local mapping of magnetic domains was performed here using a four-segmented DF4 detector of the on-axis BF/DF detector in combination with Thermo Scientific Velox software (iDPC STEM) operated in the low-magnification (LM) STEM mode. To prepare the TEM lamellae, the individual samples were polished to a mirror like finish in cross-section. Subsequently, a lamella was prepared from the edge area of the as-cast or HPT-processed disks using a ZEISS Crossbeam 340 focused ion beam (FIB) device. A Thermo Fisher Scientific FEI Themis 300 G3 S/TEM was used for imaging the magnetic domains by DPC in STEM mode. The objective lens current in LM-STEM mode is reduced to 4% which is equivalent to a magnetic field of 0.08 T. After completing all alignment steps in the LM-STEM mode with a collection angle range of 1 mrad and a beam current of 90 pA, the TEM sample was loaded and investigated.

2.4. High-precision elemental mapping

Atomically resolved elemental mapping of the HPT-processed single phase Cantor and nanocomposite HEA samples was performed using atom probe tomography (APT). For this purpose, a Local Electrode Atom Probe (LEAP 4000X HR) was used. Samples for the APT analysis were prepared from regions of interest using a ZEISS Auriga 60 FIB. The isosurfaces and proxigrams were reconstructed using a threshold value of 1.2 for the Ni/Mn ratio.
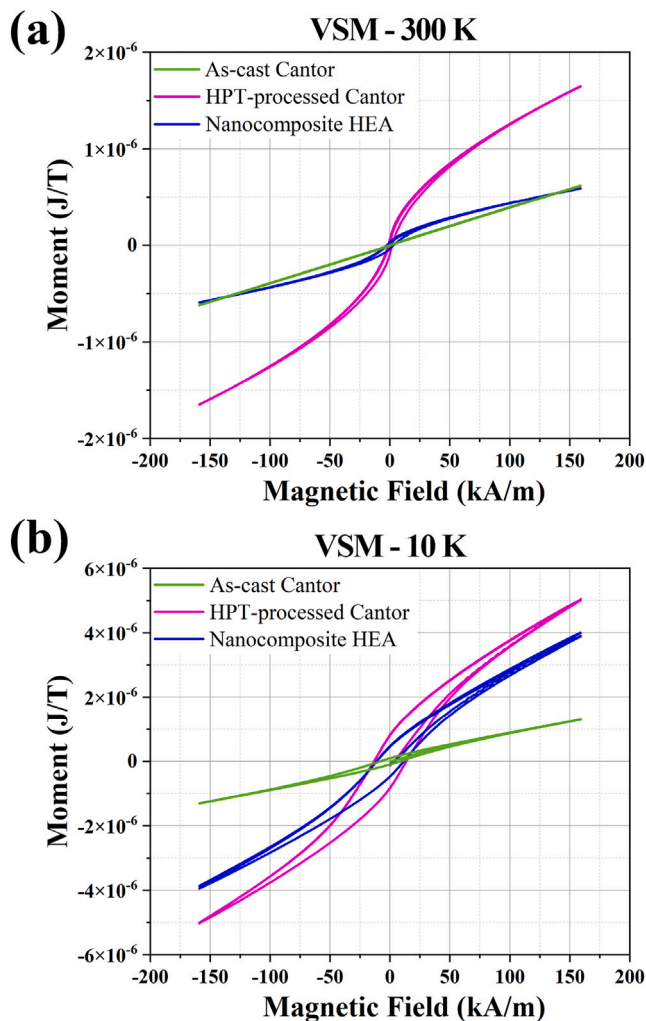
Fig. 1. VSM hysteresis loops obtained at RT (a) and 10 K (b) showing the magnetic response of the as-cast Cantor alloy, single phase HPT-processed Cantor alloy and the nanocomposite HEA produced by forced mechanical mixing of Cantor and Senkov HEAs.

3. Results

3.1. Bulk ferromagnetic properties

The ferromagnetic properties of the Cantor alloy, across different states, were comprehensively investigated employing multiple characterization techniques. The objective was to gain a deep understanding of the magnetic behavior exhibited in the different states of this particular alloy. The VSM hysteresis loops in Fig. 1 acquired at ambient temperature (RT) and 10 K demonstrate the changes in the ferromagnetic response of the as-cast Cantor and HPT-processed Cantor samples under different experimental conditions. To better present the data from this figure, the principal parameters are listed in Table 1. Fig. 1(a) characterizes the as-cast Cantor alloy as non-ferromagnetic, but a hysteresis, characteristic for ferromagnetic behavior, occurs after HPT-processing. In comparison, the nanocomposite HEA also exhibits ferromagnetic properties at RT, Fig. 1(a). However, it is worth noting that only half of the volume contributes to the measured magnetic moment in this case, as the other half is made up of the non-magnetic Senkov alloy. To account for this, the results have been normalized based on the volume fraction of the Cantor alloys in the nanocomposite HEA. When comparing the RT state across samples, the single-phase HPT-processed Cantor alloy achieves higher magnetization than the nanocomposite HEA. However, the nanocomposite HEA exhibits

relatively higher coercivity compared to the HPT-processed Cantor alloy.

Table 1 indicates that all samples exhibit enhanced ferromagnetic properties at 10 K, as shown in Fig. 1(b). The HPT-processed Cantor alloy mostly outperforms other samples in demonstrating enhanced ferromagnetic properties, including coercivity, peak magnetization at 0.2 T, and retentivity. Meanwhile, these principal values show a similar increase at 10 K compared to the RT state in the nanocomposite HEA. The peak magnetization in the nanocompoite HEA increased to nearly 2 times the estimated relative increase (in percentage) observed in the single-phase HPT-processed Cantor alloy. Conversely, the coercivity in the HPT-processed Cantor alloy shows a percentage increase that is twice that of the nanocomposite HEA. The retentivity in both HPT-processed Cantor alloy and nanocomposite HEA exhibits the similar degree of growth, as shown in Table 1. Comparing such trends does not apply to the as-cast Cantor alloy, in which the RT ferromagnetic values are negligible. [see Fig. 1(b) and Table 1].

Fig. 2 displays the results of a temperature sweep series carried out between 5 K and 300 K (RT) under constant magnetic field at 0.2 T. The as-cast Cantor alloy reveals two signal peaks that are related to transitions from the paramagnetic state to a spin glass at 75 K and to a ferromagnetic state at 30 K [17,28]. Remarkably, neither the HPT-processed Cantor alloy nor the nanocomposite show a distinct spin glass transition anymore.

3.2. Imaging magnetic domains

Fig. 3 displays DPC STEM images and EDS elemental maps acquired from the same sample. As shown by the DPC STEM micrographs in Fig. 3(a), no magnetic domains are detected in the as-cast Cantor alloy at RT. Fig. 3(b) displays the EDS elemental maps of the same region, confirming a homogeneous chemical composition for the as-cast Cantor alloy.

Fig. 4 presents a comprehensive analysis of the HPT-processed Cantor alloy, suggesting that the development of ferromagnetism in this alloy is due to the random formation of local magnetic domains with varying orientation. Fig. 4(a) displays a DPC STEM micrograph of the same sample, revealing a random orientation of the individual magnetic domains which were developed in the HPT-processed Cantor alloy. It is worth noting that the average size of coherently scattering domains (grains) identified by BF- or DF-STEM is about 30 nm, whereas the average size of magnetic domains is estimated to be about 50 nm. The single-phase crystalline nature of the HPT-processed Cantor alloy is also examined and detailed in Supplementary Materials, Fig. S1.

The corresponding EDS elemental maps in Fig. 4(b) characterize the chemical composition as being homogeneous, while the DPC STEM micrograph acquired from the same position confirms the presence of magnetic domains. This motivates a further in-depth analysis of the local chemistry to uncover facts about the origin of randomly oriented magnetic domains using APT. The nanocomposite HEA examined by VSM in Fig. 1 includes regions that match the microstructure shown in Fig. 4. However, the intermixed regions of the nanocomposite HEA appear to contribute differently to its ferromagnetic behavior, as demonstrated in Fig. 5. The DPC STEM micrographs in Fig. 5(a) demonstrate a lamellar-like orientation for the magnetic domains, which is the most significant feature concerning the formation of magnetic domains in the nanocomposite HEA. Remarkably, almost exclusively two opposite directions of the local magnetization are seen in Fig. 5(a), whereas such a magnetic texture is absent in the HPT-processed Cantor alloy, Fig. 4(a). Fig. 5(b) shows the EDS elemental maps and the corresponding DPC STEM image, indicating that such magnetic domains only exist in regions associated with the Cantor alloy composition. The relatively homogeneous distribution of oxygen in the composition renders any explanation for the magnetic domain orientation or generation based on local oxidation as unlikely. A detailed microstructural characterization of the nanocomposite HEA using high-resolution phase analysis techniques is provided in Supplementary Materials, Fig. S1.
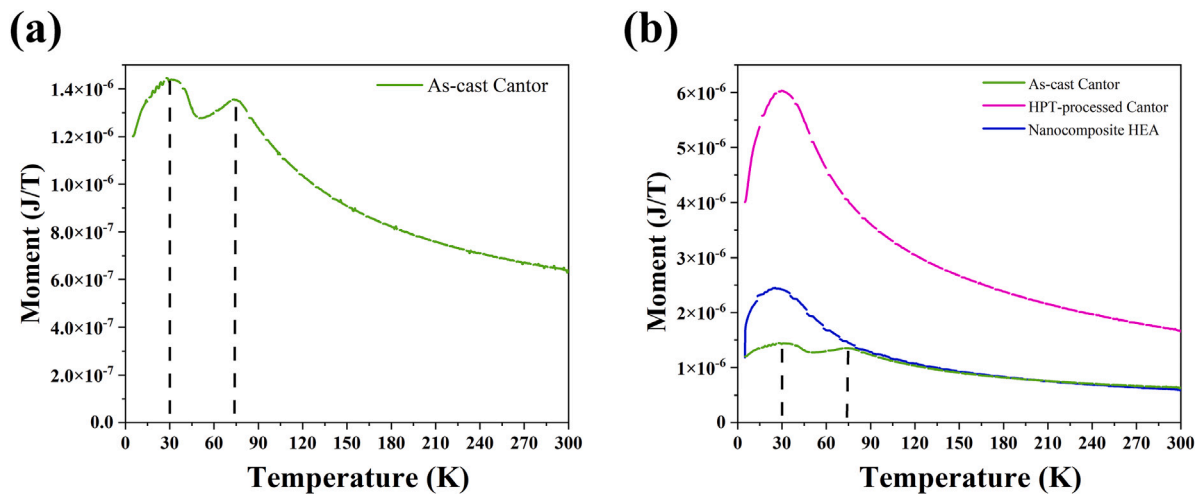
Fig. 2. A temperature sweep series carried out between 5 K and 300 K (RT) with 5 K/min while keeping the magnetic field constant at 0.2 T. (a) The magnetic phase transition for the un-deformed Cantor alloy is shown separately, as well as (b) in comparison to the HPT-processed Cantor and nanocomposite HEA.
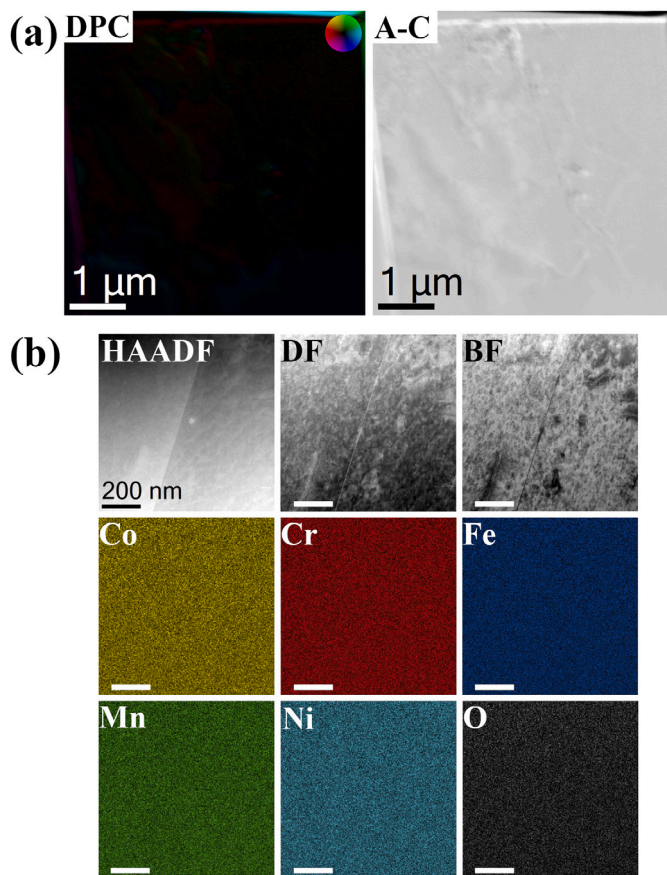

Fig. 3. (a) As-cast Cantor alloy exhibiting no evidence of ferromagnetism at room temperature (RT): magnetic induction map (left) and differential signal between opposing segments A and C (right). (b) HAADF-STEM, DF and BF images and their corresponding EDS elemental maps, confirming the homogeneous distribution of elements in the as-cast state.

3.3. High-precision elemental mapping

As depicted in Fig. 6(a), the elemental distribution in the reconstructed APT needle is consistent with the EDS maps. However, when the iso-surfaces of Ni over Mn are set to a threshold of 1.2, reflecting approximately a 10% deviation from the equiatomic composition, local Ni enrichments become apparent. This along with the corresponding proxigrams indicate the presence of Ni-enriched and Mn-depleted areas, which account for the magnetic domains observed after HPT processing of the Cantor alloy. The reconstructed APT needle in Fig. 6(b) shows the local distribution of each phase and its constituents. The iso-surfaces map, with Fe at 21%, Mn at 21% and Ni at 22%, suggests the appearance of strongly elongated regions regarding the enrichment and orientation of ferromagnetic elements such as Fe and Ni. The corresponding line scan profile, taken from the region marked by the black arrow in Fig. 6(b), reveals alternating enrichment of Ni and Co versus Fe, Mn, and Cr. This pattern is attributed to the alternating elemental enrichment of the Senkov alloy constituents. This observation suggests that Ni and Co are transported from the Cantor alloy to the regions originally occupied by the Senkov alloy, resulting in an alternating enrichment of the ferromagnetic elements. The findings shown in Fig. 5(a) align perfectly with that of Fig. 6(b), indicating that the forced mixing of the Cantor and Senkov alloys is actually element-specific. This element-specific mixing results in local enrichment of ferromagnetic Ni and Co within the Senkov alloy, while anti-ferromagnetic Cr becomes enriched at the fcc/bcc phase boundaries. The appearance of neighboring magnetic domains oriented in opposing directions with lamellar-type shape provides additional evidence supporting this analysis and interpretation [see Fig. 5(a)].

4. Discussion

HPT processing of the Cantor alloy at a hydrostatic pressure above 10 GPa or cryogenic conditions has been shown to result in the formation of a significant fraction of the hexagonal close-packed (HCP) ε-phase [29–31]. On the other hand, HPT deformation at a smaller hydrostatic pressure and ambient conditions has often been reported to maintain the single phase (random solid solution) state of the Cantor alloy [29,32–34]. Even employing precise local methods such as STEM-EDS and APT for examining the microstructural characteristics of as-deformed CoCrFeMnNi HEA confirmed a consistent presence of a uniform solid solution under such conditions [34]. The specific magnetic properties of HPT-processed Cantor alloy, as confirmed by VSM and STEM DPC analyses, present challenges to microscopic investigations and suggests a need for more intricate examination. The combination of comprehensive bulk magnetic measurements and direct observation of magnetic domains using STEM DPC provides valuable insights for subsequent APT analysis and calls for the exploration of potentially hidden correlations in the element distributions. Without
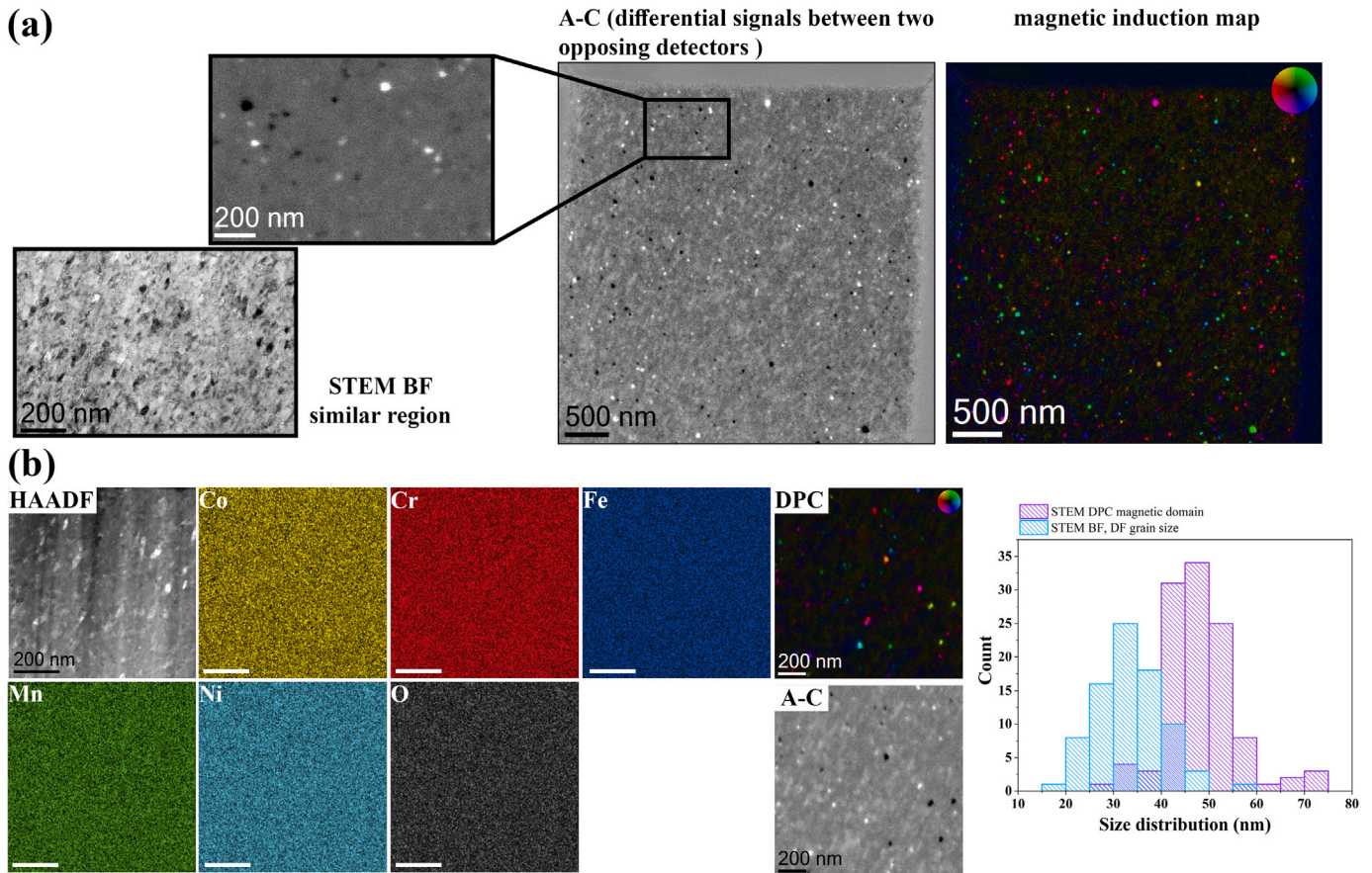
Fig. 4. The origin of ferromagnetic properties investigated by DPC STEM and STEM EDS elemental mapping. (a) The HPT-processed Cantor alloy displays randomly oriented magnetic domains at random locations, and the BF-STEM micrograph from a similar position shows that the grains imaged in Bragg condition do not coincide with the magnetic domains. (b) STEM EDS elemental mapping and the corresponding DPC STEM micrograph of the identical region indicate no observable element enrichment within the resolution of this analysis. Furthermore, the estimated average grain size and magnetic domain size (right panel in (b)) imply that there is no immediate correlation between the magnetic domains and the grains.
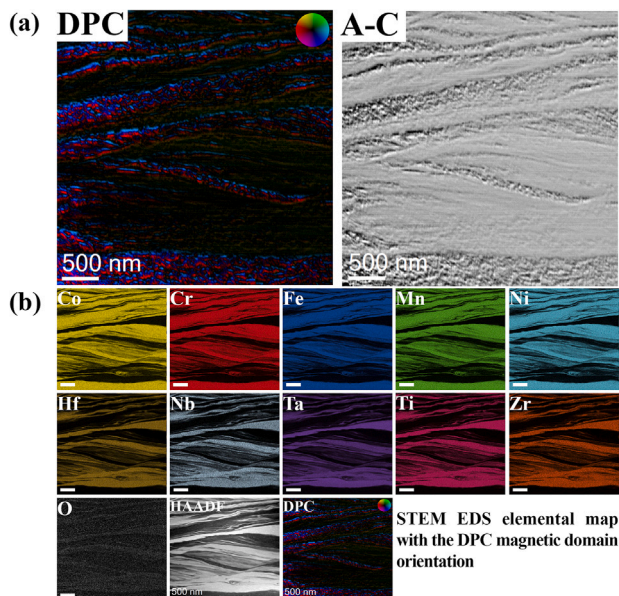

Fig. 5. (a) DPC STEM micrographs of the HPT-processed nanocomposite HEA showing the intermixed region: magnetic induction map (left) and the differential signal of the opposing detector segments A and C (right). (b) EDS elemental maps of the same region.

such findings, an APT-driven analytical approach would lack statistical significance and relevance.

The deviations from a completely random solid solution in the HPT-processed Cantor alloy, as indicated by the STEM DPC measurements in Fig. 4, require further exploration. Previous examinations using STEM EDS and preliminary APT assessments did not show any signs of phase separation or decomposition, seemingly confirming a single phase, see Supplementary Materials, Fig. S1, and random solid solution state. The post-deformation heat treatment of both HPT-processed Cantor and nanocomposite HEA at 953 K for 20 min results in phase decomposition, leading to the formation of distinct Cr-rich and Mn-rich precipitates. This treatment enhances the material's ferromagnetic behavior at cryogenic temperatures, aligning with and slightly amplifying the general findings of this study, see Supplementary Materials, Fig. S2 and S3.

Although the primary focus of this work is identifying subtle microstructural changes in the as-deformed state, it is crucial to acknowledge that these findings are directly influenced by the specific methodology employed. This study integrates STEM DPC, STEM EDS, and APT to gain a comprehensive understanding of the complexities of material behavior. The discrepancy between the STEM EDS results displayed by Figs. 4(b) and 5(b) and the APT cluster analysis results in Fig. 6 arises from the projection effect in S/TEM. While STEM EDS data collection relies upon the electron beam passing through the entire sample, it produces an averaged composition that can obscure signals from localized element enrichments like Ni. In contrast, APT achieves near atomic-scale, three-dimensional reconstruction through analysis of the mass spectrum of each atom, eliminating projection effects.
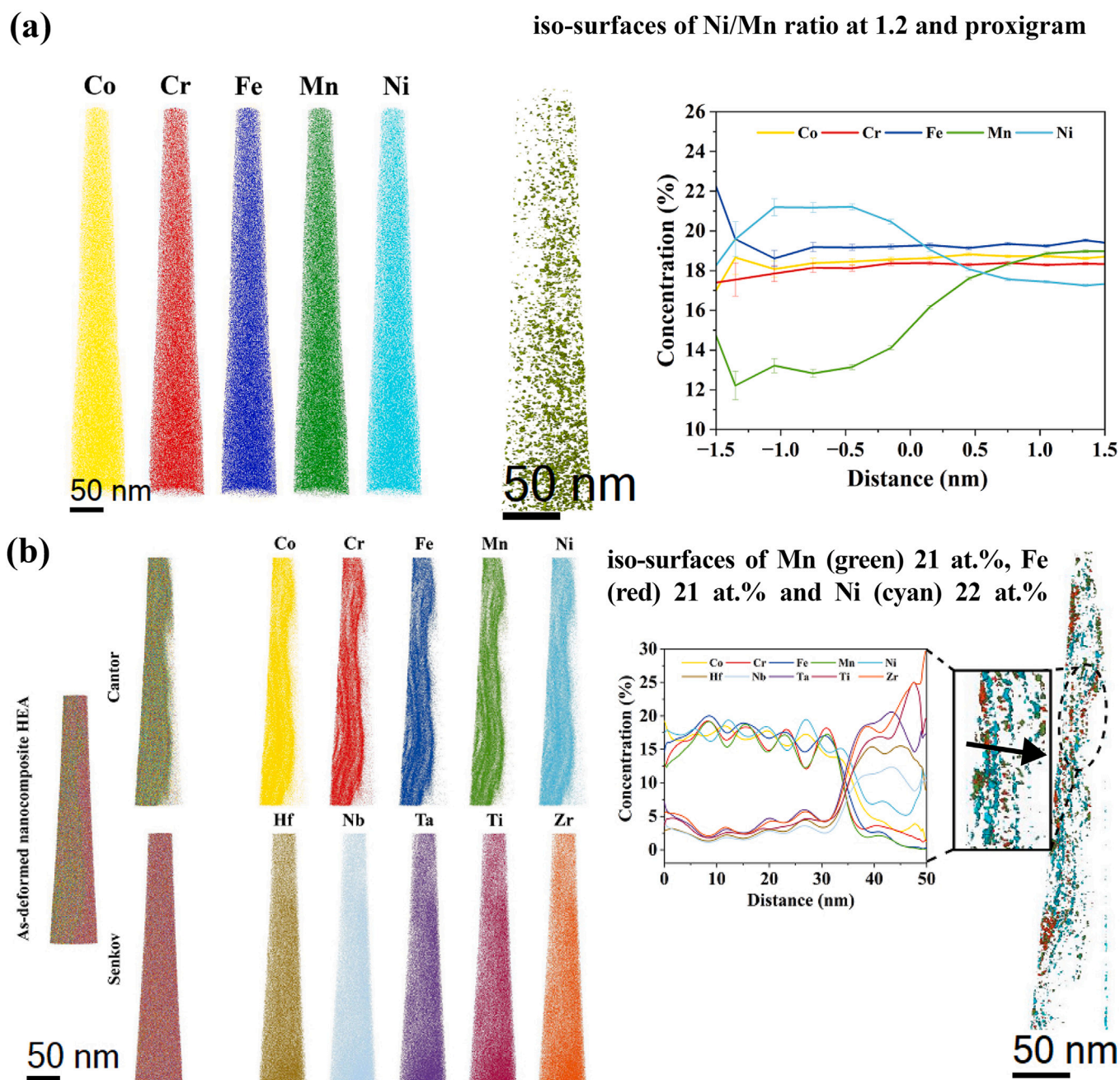
Fig. 6. (a) APT results show the iso-surface maps of the reconstructed needles of the HPT-processed Cantor alloy, along with the corresponding proxigram that reveals a local enrichment of Ni. (b) The atomic scale 3-D reconstruction of the nanocomposite HEA with iso-surfaces map displaying Mn-, Fe-, and Ni-enriched regions.

This enables precise spatial mapping and accurate detection of local concentrations, even in small regions.

4.1. Deformation-induced ferromagnetism

Fig. 3(b) demonstrates that the as-cast Cantor alloy features a uniform solid solution, which remains unchanged even upon further investigation with atomic scale resolution [35]. The observations presented in Figs. 4 and 6(a) support the hypothesis that the transition [11] from the paramagnetic to a soft ferromagnetic state in the Cantor alloy is attributed to the deformation-induced formation of Ni-rich regions [4].

Fig. 4 shows that the average size of magnetic domains observed by DPC STEM is larger than the average grain size obtained from the BF-

and DF-STEM micrographs, excluding that such contrasts in DPC STEM arise purely from diffraction features. This is further corroborated by the data, which suggests that multiple small grains can belong to the same magnetic domain, similar to when one large grain contains multiple domains [36]. The samples exhibit an improved ferromagnetic behavior at 10 K due to factors that give rise to ferromagnetic metals demonstrating higher magnetic coercivity at low temperatures [37]. Since the thermal energy is inadequate to randomize the orientation of the local magnetic moments, a greater effective magnetic moment and smaller magnetic domains emerge, and this in turn makes it more energetically demanding to alter domain orientation [38]. HPT processing enhances coercivity due to the strain-induced magnetic anisotropy [39]. Together with increased dislocation density, grain shape anisotropy and residual strain distributions serve to enhance

the propensity for magnetic domain wall pinning [40,41]. As a consequence, both HPT-processed samples show superior and relatively comparable magnetic hardness at 10 K in comparison to that of the un-deformed Cantor alloy [39]. The peak magnetization at 0.2 T in the HPT-processed Cantor material is exceptionally high due to its initial superiority over all other samples in the RT state. On the other hand, the nanocomposite HEA shows a threefold increase at a temperature of 10 K. This significant improvement is attributed to the remarkably reduced grain size in the nanolaminates compared to the single phase HPT-processed Cantor material [33]. Consequently, this reduction greatly enhances the likelihood of magnetic wall pinning, resulting in the formation of magnetic wall domains that are both smaller in size and more versatile in their orientations. At higher temperatures the thermal energy surpasses the magnetic field energy, allowing domains to expand, yet not inducing misalignment of local moments [36].

Thus, there is an involved interplay of magnetic domain size and the grain size, determined as coherently scattering domain size. As the grain size decreases, coercivity increases until the grain size becomes equal to the domain size, known as the "critical grain size" [42,43]. Beyond this point, if the grain size continues to decrease, domain rotation occurs instead of domain wall motion, leading to a decrease in coercivity below the critical size. Therefore, at these smaller sizes, the domain wall motion is likely not a factor.

4.2. Enhanced tuning of the magnetic domains by co-deformation

The lamellar-like orientation of magnetic domains in the nanocomposite HEA, as illustrated in Figs. 5 and 6(b), originates from the alternating phase separation or local enrichment [44] of the Cantor alloy's ferromagnetic constituents, driven by SPD. The element-specific phase separation shown by the APT results in Fig. 6(b) is facilitated by the co-deformation of Cantor and Senkov alloys. This, in turn, has resulted in the formation of lamellar-like magnetic domains containing elements such as Ni and Co, which couple ferromagnetically. Meanwhile, the adjacent phase is enriched with Cr, exhibiting antiferromagnetic behavior [45]. As a result, despite the remarkably enhanced phase separation in the nanocomposite HEA, the HPT-processed Cantor alloy exhibits higher coercivity and peak magnetization in comparison, indicating a greater resistance to a change of its magnetization.

4.3. Manifestations of the cocktail effect

In the case of HPT-processed Cantor alloy, local enrichment of ferromagnetic elements is responsible for the formation of highly localized and randomly oriented magnetic domains. This could be explained by the fact that SPD can expedite the development of precipitates or enriched regions by subjecting the material to high strain rates and large plastic strains [29]. When the material undergoes deformation, the varying energy levels across different lattice sites impede the motion of dislocations and cause them to accumulate at favorable locations. Consequently, this drives the system closer to a metastable equilibrium state with reduced free enthalpy. In conjunction with the dislocations and GBs serving as pathways for diffusion, there is ample potential to enhance the diffusion rate of atoms, especially via deformation-induced point defects or higher-order defects serving as short-circuit paths for atomic transport [46,47]. Furthermore, the elevated density of dislocations provides additional sites for the formation of precipitates [48]. Moreover, the increased fraction of GBs resulting from grain refinement acts as preferential sites for precipitation or enrichment due to their higher energy and augmented diffusion rates.

The deformation-stimulated formation of Ni-rich and Cr-rich particles correlates with the known tendency of the Cantor alloy to decompose with the formation of a Cr-rich sigma phase together with NiMn- or FeCo-rich precipitates [49–51]. According to the effective temperature concept [52,53], the HPT processing at RT is equivalent to annealing the material at a higher temperature, T_{eff} provoking formation of the corresponding phases that are stable under these conditions. The present finding, if they are treated within the framework of the effective temperature concept, indicate that T_{eff} is less than 600 °C to 700 °C.

The 'cocktail effect' manifests when elements with high diffusion rates and ferromagnetic properties, initially in a state of equilibrium, are subjected to deformation. This deformation creates diffusion paths through dislocation cores and high-angle GBs. As a result, the alloy's paramagnetic state, which is primarily maintained by its high compositional entropy, is disrupted. Thermodynamics drives the alloy to decomposition that is supported by enhanced diffusion rates, leading to the formation of precipitates (including metastable or non-equilibrium ones). By introducing a second phase, which in this case is the Senkov alloy, deformation-induced amorphization of the bcc phase occurs together with dislocation accumulation and enrichment of solutes at the phase boundaries [33]. In such scenarios, elements that exhibit a stronger attraction to the constituents of the neighboring phase will find it energetically favorable to diffuse into the Senkov alloy. The resulting phase separation, driven by the cocktail effect, occurs when the Senkov alloy and its constituents are present [33]. Note that whereas the diffusion rates of solutes in fcc matrices are typically not too different (diffusion of $3d$ elements in pure Al is though a most exciting exception [54]), the corresponding diffusion rates in bcc matrices could vary over many orders of magnitude [55]. Thus, the bcc Senkov alloy triggers a phase separation within the fcc Cantor alloy filtering effectively the "slow" and "fast" diffusing components.

5. Conclusions

Our study has shown that HPT-processing of HEAs leads to a transition from paramagnetic to ferromagnetic states at ambient conditions. The observed deformation-induced ferromagnetism can be comprehended in terms of the 'cocktail effect', advocated for HEAs, in which the formation of ferromagnetic particles is attributed to element-selective deformation-induced atomic migration and local enrichment of ferromagnetic elements.

Two different routes for inducing ferromagnetism are explored; first, by deforming the Cantor alloy as a single-phase disk and second, by co-deformation and forced mechanical mixing of the Cantor alloy with a non-ferromagnetic HEA such as the Senkov alloy. Both approaches lead to a pronounced ferromagnetic response. However, the co-deformation route involved the formation of anisotropies of the microstructure and the spatial distribution of ferromagnetic and antiferromagnetic elements, which led to the formation of ferromagnetic regions with aligned magnetization in contrast to the deformed single-phase material.

The main findings of this study are:

- The as-cast Cantor alloy exhibits two phase transitions upon cooling; that is, a spin glass transition at 70 K and a ferromagnetic transition at 30 K. This is in agreement with earlier findings [17]. However, the HPT-processed Cantor does not exhibit a spin glass transition anymore, showing instead a more pronounced ferromagnetic transition. In comparison with the un-deformed Cantor and nanocomposite HEA, the HPT-processed Cantor also displays a higher magnetic moment at elevated temperatures.
- While the nanocomposite HEA exhibits a remarkable degree of phase separation attributed to the co-deformation process, the peak magnetization for this material is lower in comparison to the HPT-processed Cantor alloy. As a consequence of the pronounced phase separation, lamellar-like alignments of ferromagnetic NiCo-rich and anti-ferromagnetic Cr-rich domains form, which reduce the overall magnetic moment in the nanocomposite HEA. The absence of such a phenomenon in the HPT-processed Cantor alloy gives rise to a comparable coercivity in this sample.

- Deformation-induced changes of the local chemical composition transform the Cantor alloy into a soft ferromagnetic material. Furthermore, grain refinement, together with increased dislocation density, produces randomly oriented magnetic domains at random positions. This combination of local Ni-enriched particles with refined grains results in a higher peak magnetization of the HPT-processed Cantor alloy.

These findings may pave the way for the development of new magnetic materials with tailored properties for various applications.

CRediT authorship contribution statement

Shabnam Taheriniya: Writing – review & editing, Writing – original draft, Visualization, Investigation, Formal analysis, Data curation. **Reshma Sonkusare:** Data curation. **Torben Boll:** Validation, Data curation. **Sergiy V. Divinski:** Writing – review & editing, Supervision. **Martin Peterlechner:** Methodology, Investigation, Data curation. **Harald Rösner:** Writing – review & editing, Supervision, Project administration, Methodology, Investigation, Conceptualization. **Gerhard Wilde:** Writing – review & editing, Supervision, Funding acquisition.

Declaration of competing interest

The authors declare that they have no known competing financial interests or personal relationships that could have appeared to influence the work reported in this paper.

Acknowledgments

Appendix A. Supplementary data

Supplementary material related to this article can be found online at https://doi.org/10.1016/j.actamat.2024.120421.

References

[1] Oliver Gutfleisch, Matthew A Willard, Ekkes Brück, Christina H Chen, S.G. Sankar, J. Ping Liu, Magnetic materials and devices for the 21st century: stronger, lighter, and more energy efficient, Adv. Mater. 23 (7) (2011) 821–842.

[2] Easo P. George, Dierk Raabe, Robert O. Ritchie, High-entropy alloys, Nat. Rev. Mater. 4 (8) (2019) 515–534.

[3] Xin Wang, Wei Guo, Yongzhu Fu, High-entropy alloys: emerging materials for advanced functional applications, J. Mater. Chem. A 9 (2021) 663–701.

[4] X.F. Wang, Yong Zhang, Yi Qiao, G.L. Chen, Novel microstructure and properties of multicomponent cocrcufenitix alloys, Intermetallics 15 (3) (2007) 357–362.

[5] S. Maiti, Discovery of a superconducting high-entropy alloy, Phys. Rev. Lett. 113 (10) (2014) 107001.

[6] Michael C. Gao, Jien-Wei Yeh, Peter K. Liaw, Yong Zhang, High-Entropy Alloys: Fundamentals and Applications, Springer Cham, 2018.

[7] Jien-Wei Yeh, Su-Jien Lin, Breakthrough applications of high-entropy materials, J. Mater. Res. 33 (2018) 3129–3137.

[8] Sheetal Kumar Dewangan, Ananddev Mangish, Sunny Kumar, Ashutosh Sharma, Byungmin Ahn, Vinod Kumar, A review on High-Temperature Applicability: A milestone for high entropy alloys, Eng. Sci. Technol. Int. J. 35 (2022) 101211.

[9] Bruno G.F. Eggert, Erna K. Delczeg-Czirjak, Fernando Maccari, Susmit Kumar, Oliver Gutfleisch, Helmer Fjellvåg, Bjørn C. Hauback, Christoph Frommen, Exploring V-Fe-Co-Ni-Al and V-Fe-Co-Ni-Cu high entropy alloys for magnetocaloric applications, J. Alloys Compd. 921 (2022) 166040.

[10] Jiro Kitagawa, Masaki Fukuda, Satoshi Fukuda, Kenta Fujiki, Yuki Nakamura, Terukazu Nishizaki, Discovery of ferromagnetism in new multicomponent alloy Ti–Nb–Cr–Ru, APL Mater. 10 (7) (2022).

[11] B.G.F. Eggert, E.K. Delczeg-Czirjak, B.C. Hauback, C. Frommen, Magnetic transitions in V-Fe-Co-Ni-Cu-based high entropy alloys, Mater. Today Phys. 35 (2023) 101116.

[12] S. Ranganathan, Alloyed pleasures: Multimetallic cocktails, Curr. Sci. 85 (2003) 1404–1406.

[13] E.J. Pickering, N.G. Jones, High-entropy alloys: a critical assessment of their founding principles and future prospects, Int. Mater. Rev. 61 (3) (2016) 183–202.

[14] B.X. Cao, C. Wang, T. Yang, C.T. Liu, Cocktail effects in understanding the stability and properties of face-centered-cubic high-entropy alloys at ambient and cryogenic temperatures, Scr. Mater. 187 (2020) 250–255.

[15] D.B. Miracle, High-entropy alloys: A current evaluation of founding ideas and core effects and exploring nonlinear alloys, JOM 69 (2017) 2130–2136.

[16] E. Menéndez, J. Sort, M.O. Liedke, J. Fassbender, S. Surinach, M.D. Baró', J. Nogués, Two-fold origin of the deformation-induced ferromagnetism in bulk fe60al40 (at.%) alloys, New J. Phys. 10 (2008) 103030.

[17] Oldřich Schneeweiss, Martin Friák, Marie Dudová, David Holec, Mojmír Šob, Dominik Kriegner, Václav Holỳ, Přemysl Beran, Easo P. George, Jörg Neugebauer, et al., Magnetic properties of the crmnfeconi high-entropy alloy, Phys. Rev. B 96 (1) (2017) 014437.

[18] Xiaohong Li, Li Lou, Wenpeng Song, Guangwei Huang, Fuchen Hou, Qian Zhang, Hai-Tian Zhang, Jianwei Xiao, Bin Wen, Xiangyi Zhang, Novel bimorphological anisotropic bulk nanocomposite materials with high energy products, Adv. Mater. 29 (16) (2017) 1606430.

[19] Maogang Gong, Alec Kirkeminde, Manfred Wuttig, Shenqiang Ren, Phase transformation-induced tetragonal feco nanostructures, Nano Lett. 14 (11) (2014) 6493–6498, PMID: 25268222.

[20] Guangwei Huang, Xiaohong Li, Li Lou, Yingxin Hua, Guangjun Zhu, Ming Li, Hai-Tian Zhang, Jianwei Xiao, Bin Wen, Ming Yue, Xiangyi Zhang, Engineering bulk, layered, multicomponent nanostructures with high energy density, Small 14 (22) (2018) 1800619.

[21] J.N. Chapman, The investigation of magnetic domain structures in thin foils by electron microscopy, J. Phys. D: Appl. Phys. 17 (4) (1984) 623.

[22] J.N. Chapman, I.R. McFadyen, S. McVitie, Modified differential phase contrast lorentz microscopy for improved imaging of magnetic structures, IEEE Trans. Magn. 26 (5) (1990) 1506–1511.

[23] J.N. Chapman, M.R. Scheinfein, Transmission electron microscopies of magnetic microstructures, J. Magn. Magn. Mater. 200 (1–3) (1999) 729–740.

[24] A. Lubk, J. Zweck, Differential phase contrast: An integral perspective, Phys. Rev. A 91 (2) (2015) 023805.

[25] S. Majert, H. Kohl, High-resolution stem imaging with a quadrant detector—conditions for differential phase contrast microscopy in the weak phase object approximation, Ultramicroscopy 148 (2015) 81–86.

[26] Andreas Hütten, Daniela Ramermann, Björn Büker, Andreas Becker, Inga Ennen, Robert Webster, Stephen McVitie, T.P. Almeida, Imaging microstructural impact on magnetic behavior, Imaging (2021).

[27] Takehito Seki, Yuichi Ikuhara, Naoya Shibata, Toward quantitative electromagnetic field imaging by differential-phase-contrast scanning transmission electron microscopy, Microscopy 70 (1) (2021) 148–160.

[28] P. Koželj, S. Vrtnik, M. Krnel, A. Jelen, D. Gačnik, M. Wencka, Z. Jagličić, A. Meden, G. Dražić, F. Danoix, J. Ledieu, M. Feuerbacher, J. Dolinšek, Spin-glass magnetism of the non-equiatomic CoCrFeMnNi high-entropy alloy, J. Magn. Magn. Mater. 523 (2021) 167579.

[29] Boris B. Straumal, Roman Kulagin, Brigitte Baretzky, Natalia Yu Anisimova, Mikhail V. Kiselevskiy, Leonid Klinger, Petr B. Straumal, Olga A. Kogtenkova, Ruslan Z. Valiev, Severe plastic deformation and phase transformations in high entropy alloys: A review, Crystals 12 (1) (2022).

[30] Robert Chulist, Aurimas Pukenas, Paul Chekhonin, Anton Hohenwarter, Reinhard Pippan, Norbert Schell, Werner Skrotzki, Phase transformation induced by high pressure torsion in the high-entropy alloy CrMnFeCoNi, Materials 15 (23) (2022).

[31] Werner Skrotzki, Robert Chulist, Severe plastic deformation of high-entropy alloys, Mater. Trans. 64 (8) (2023) 1769–1783.

[32] B. Schuh, F. Mendez-Martin, B. Völker, E.P. George, H. Clemens, R. Pippan, A. Hohenwarter, Mechanical properties, microstructure and thermal stability of a nanocrystalline CoCrFeMnNi high-entropy alloy after severe plastic deformation, Acta Mater. 96 (2015) 258–268.

[33] Shabnam Taheriniya, Farnaz A. Davani, Sven Hilke, Marco Hepp, Christian Gadelmeier, Mohammed.Reda Chellali, Torben Boll, Harald Rösner, Martin Peterlechner, Christoph Gammer, Sergiy V. Divinski, Benjamin Butz, Uwe Glatzel, Horst Hahn, Gerhard Wilde, High entropy alloy nanocomposites produced by high pressure torsion, Acta Mater. 208 (2021) 116714.

[34] Benjamin Schuh, Inas Issa, Timo Müller, Thomas Kremmer, Christoph Gammer, Reinhard Pippan, Anton Hohenwarter, Deformation Induced Structure and Property Changes in a Nanostructured Multiphase CrMnFeCoNi High-Entropy Alloy, Nanomaterials 13 (5) (2023).

[35] M. Vaidya, K.G. Pradeep, B.S. Murty, G. Wilde, S.V. Divinski, Radioactive isotopes reveal a non sluggish kinetics of grain boundary diffusion in high entropy alloys, Sci. Rep. 7 (1) (2017) 12293.

[36] Robert C. O'Handley, Modern Magnetic Materials: Principles and Applications, Wiley, 1999.

[37] Yuan-Yuan Tan, Zhong-Jun Chen, Ming-Yao Su, Gan Ding, Min-Qiang Jiang, Zhou-Can Xie, Yu Gong, Tao Wu, Zhong-Hua Wu, Hai-Ying Wang, Lan-Hong Dai, Lattice distortion and magnetic property of high entropy alloys at low temperatures, J. Mater. Sci. Technol. 104 (2022) 236–243.

[38] Amitesh Paul, Xiaojing Liu, Megumi Kawasaki, Klaus-Dieter Liss, Inverted magnetic response in severe plastically deformed nanostructured high-entropy alloy, Appl. Phys. Lett. 122 (2023) 052402.

[39] Deli Kong, András Kovács, Michalis Charilaou, Fengshan Zheng, Lihua Wang, Xiaodong Han, Rafal E. Dunin-Borkowski, Direct observation of tensile-strain-induced nanoscale magnetic hardening, Nature Commun. 14 (1) (2023) 3963.

[40] Hansheng Chen, Fan Yun, Jiangtao Qu, Yingfei Li, Zhenxiang Cheng, Ruhao Fang, Zhixiao Ye, Simon P. Ringer, Rongkun Zheng, Coercivity degradation caused by inhomogeneous grain boundaries in sintered Nd–Fe–B permanent magnets, Phys. Rev. Mater. 2 (2018) 054404.

[41] Kristina Žagar Soderžnik, Kristina Žužek Rožman, Matej Komelj, András Kovács, Patrick Diehle, Thibaud Denneulin, Aleksei Savenko, Marko Soderžnik, Spomenka Kobe, Rafal E. Dunin-Borkowski, Joachim Mayer, Boštjan Markoli, Sašo Šturm, Microstructural insights into the coercivity enhancement of grain-boundary-diffusion-processed Tb-treated Nd-Fe-B sintered magnets beyond the core–shell formation mechanism, J. Alloys Compd. 864 (2021) 158915.

[42] A.R. Muxworthy1, W. Williams, Critical superparamagnetic/single-domain grain sizes in interacting magnetite particles: implications for magnetosome crystals, J. R. Soc. Interface 6 (2009) 1207–1212.

[43] Q. Li, C.W. Kartikowati, S. Horie, T. Ogi, T. Iwaki, K. Okuyama, Correlation between particle size/domain structure and magnetic properties of highly crystalline Fe3O4 nanoparticles, Sci. Rep. 7 (2017) 9894.

[44] Rui feng Zhao, Bo Ren, Elemental synergistic effect in coxcrcufemnni high-entropy alloys and its influence on phase and magnetic properties, J. Mater. Res. Technol. 1 (2023).

[45] Timothy A. Elmslie, Jacob Startt, Sujeily Soto-Medina, Yang Yang, Keke Feng, Ryan E. Baumbach, Emma Zappala, Gerald D. Morris, Benjamin A. Frandsen, Mark W. Meisel, Michele V. Manuel, Rémi Dingreville, James J. Hamlin, Magnetic properties of equiatomic crmnfeconi, Phys. Rev. B 106 (2022) 014418.

[46] Gerhard Wilde, Sergiy Divinski, Grain boundaries and diffusion phenomena in severely deformed materials, Mater. Trans. 60 (7) (2019) 1302–1315.

[47] Gerhard Wilde, Harald Rösner, Sergiy Divinski, Internal interfaces in severely deformed metals and alloys: Coupling of kinetics, structure and strain with properties and performance, Mater. Trans. 64 (7) (2023) 1331–1345.

[48] Shabnam Taheriniya, Nuri Choi, Sangsun Yang, Reshma Sonkusare, Ji.Hun Yu, Jai-Sung Lee, Harald Rösner, Martin Peterlechner, Torben Boll, Christoph Gammer, et al., Additively manufactured equiatomic cocrfemnni high entropy alloy: Precipitation-induced heterogeneity by mechano-chemical coupling, J. Alloys Compd. 938 (2023) 168514.

[49] F. Otto, A. Dlouhý, K.G. Pradeep, M. Kuběnová, D. Raabe, G. Eggeler, E.P. George, Decomposition of the single-phase high-entropy alloy CrMnFeCoNi after prolonged anneals at intermediate temperatures, Acta Mater. 112 (2016) 40–52.

[50] Guillaume Bracq, Mathilde Laurent-Brocq, Loïc Perrière, Rémy Pirès, Jean-Marc Joubert, Ivan Guillot, The fcc solid solution stability in the Co-Cr-Fe-Mn-Ni multi-component system, Acta Mater. 128 (2017) 327–336.

[51] Kap Ho Lee, Soon-Ku Hong, Sun Ig Hong, Precipitation and decomposition in CoCrFeMnNi high entropy alloy at intermediate temperatures under creep conditions, Materialia 8 (2019) 100445.

[52] B. Straumal, A. Korneva, P. Zieba, Phase transitions in metallic alloys driven by the high pressure torsion, Arch. Civ. Mech. Eng. 14 (2) (2014) 242–249.

[53] Boris B. Straumal, Olga A. Kogtenkova, Ruslan Z. Valiev, Pawel Zieba, Brigitte Baretzky, Diffusion and phase transitions accelerated by severe plastic deformation, Diffusion Found. 5 (2015) 95–108.

[54] H. Mehrer, Diffusion in Solids. Fundamentals, Methods, Materials, Diffusion-Controlled Processes, Springer, 2007.

[55] Aloke Paul, Tomi Laurila, Vesa Vuorinen, Sergiy V. Divinski, Thermodynamics, Diffusion and the Kirkendall Effect in Solids, Springer, 2014.